JACS
JOURNAL OF THE AMERICAN CHEMICAL SOCIETY
Article
pubs.acs.org/JACS

A >200 meV Uphill Thermodynamic Landscape for Radical Transport in *Escherichia coli* Ribonucleotide Reductase Determined Using Fluorotyrosine-Substituted Enzymes

Kanchana R. Ravichandran,[†] Alexander T. Taguchi,[†] Yifeng Wei,[†] Cecilia Tommos,[§] Daniel G. Nocera,*[,⊥] and JoAnne Stubbe*[,†,‡]

[†]Department of Chemistry and [‡]Department of Biology, Massachusetts Institute of Technology, 77 Massachusetts Avenue, Cambridge, Massachusetts 02139, United States

[§]Department of Biochemistry and Biophysics, University of Pennsylvania, Philadelphia, Pennsylvania 19104, United States

[⊥]Department of Chemistry and Chemical Biology, Harvard University, 12 Oxford Street, Cambridge, Massachusetts 02138, United States

Supporting Information

ABSTRACT: *Escherichia coli* class Ia ribonucleotide reductase (RNR) converts ribonucleotides to deoxynucleotides. A diferric-tyrosyl radical (Y_{122}•) in one subunit (β2) generates a transient thiyl radical in another subunit (α2) via long-range radical transport (RT) through aromatic amino acid residues (Y_{122} ⇆ [W_{48}] ⇆ Y_{356} in β2 to Y_{731} ⇆ Y_{730} ⇆ C_{439} in α2). Equilibration of Y_{356}•, Y_{731}•, and Y_{730}• was recently observed using site specifically incorporated unnatural tyrosine analogs; however, equilibration between Y_{122}• and Y_{356}• has not been detected. Our recent report of Y_{356}• formation in a kinetically and chemically competent fashion in the reaction of β2 containing 2,3,5-trifluorotyrosine at Y_{122} (F_3Y_{122}•-β2) with α2, CDP (substrate), and ATP (effector) has now afforded the opportunity to investigate equilibration of F_3Y_{122}• and Y_{356}•. Incubation of F_3Y_{122}•-β2, Y_{731}F-α2 (or Y_{730}F-α2), CDP, and ATP at different temperatures (2−37 °C) provides $\Delta E^{\circ\prime}$(F_3Y_{122}•−Y_{356}•) of 20 ± 10 mV at 25 °C. The pH dependence of the F_3Y_{122}• ⇆ Y_{356}• interconversion (pH 6.8−8.0) reveals that the proton from Y_{356} is in rapid exchange with solvent, in contrast to the proton from Y_{122}. Insertion of 3,5-difluorotyrosine (F_2Y) at Y_{356} and rapid freeze-quench EPR analysis of its reaction with Y_{731}F-α2, CDP, and ATP at pH 8.2 and 25 °C shows F_2Y_{356}• generation by the native Y_{122}•. F_nY-RNRs (n = 2 and 3) together provide a model for the thermodynamic landscape of the RT pathway in which the reaction between Y_{122} and C_{439} is ∼200 meV uphill.

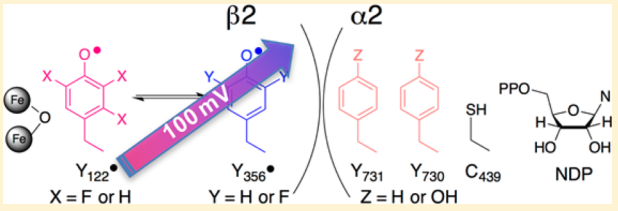

INTRODUCTION

The *E. coli* class Ia ribonucleotide reductase (RNR) contains two homodimeric subunits, α2 and β2, and functions as an $\alpha2\beta2$ complex.[1,2] Its active cofactor is a diferric-tyrosyl radical (Y_{122}•) unit buried within β2. This cofactor generates a transient thiyl radical (C_{439}•) in α2[3,4] which initiates reduction of the four nucleotides (CDP, GDP, ADP, and UDP) to their corresponding 2′-deoxynucleotides (dNDP), with the specificity of reduction dictated by the appropriate allosteric effector (ATP, TTP, dGTP, and dATP).[5−8] During each turnover, Y_{122}• reversibly oxidizes C_{439} via multiple proton-coupled electron transfer (PCET) steps through a pathway involving aromatic amino acid residues Y_{122} ⇆ [W_{48}] ⇆ Y_{356} in β2 to Y_{731} ⇆ Y_{730} ⇆ C_{439} in α2. Currently, there is no direct evidence for the involvement of W_{48} in RT.[9−11] In the wild-type (wt) RNR, only Y_{122}• is observed in the presence of substrates (S) and effectors (E); there has been no detectable electron delocalization over the other pathway tyrosines.[12] In this paper, we present the first insight into the thermodynamic landscape of the RT pathway within β2. Site-specific replacement of either Y_{122} or Y_{356} with fluorotyrosines (F_nY, n = 2 and 3) in combination with pathway-blocked α2 mutants (Y_{731}F-α2 or Y_{730}F-α2)/CDP/ATP and X-band electron paramagnetic resonance (EPR) spectroscopy[13] provides evidence for equilibration of Y_{122}• with Y_{356}• as a function of temperature and pH. These studies have allowed estimation of $\Delta E^{\circ\prime}$(Y_{356}•−Y_{122}•) of ∼100 mV.

Detection of low concentrations of any pathway radical in the wt RNR system is challenging due to rate-limiting conformational changes and the substantial overlap in the EPR spectra of the Y•'s.[14] Initial attempts to address if Y_{122}• equilibrated with the pathway tyrosines (Y_{356}, Y_{731}, and Y_{730}) utilized the ability to collapse the Y• doublet EPR spectrum into a singlet with β-methylene-deuterated ([β-$^2H_2$]) Y's.[12,14] β2 containing globally incorporated [β-$^2H_2$]Y's was reacted with α2 containing protonated Y's, dCDP, and TTP.[12] These conditions promote $\alpha2\beta2$ complex formation[1] but prevent turnover, thus potentially allowing equilibration of the pathway Y•'s. Unfortunately, no

Received: August 6, 2016
Published: September 20, 2016

DOI: 10.1021/jacs.6b08200
J. Am. Chem. Soc. 2016, 138, 13706−13716

unlabeled Y• signal could be detected; the EPR spectrum of Y• in the $\alpha2\beta2$ complex was identical to that in free $\beta2$.[12]

Recently, we showed that the reaction of NO_2Y_{122}•-$\beta2$ (3-nitrotyrosine at position 122), which is predicted to be 200 mV more difficult to oxidize than Y at pH 7.0,[15,16] with wt-$\alpha2$, CDP, and ATP generates a new Y•, localized to Y_{356}.[17] Using 3,5-difluorotyrosine (F_2Y) at Y_{731} (or Y_{730}) we demonstrated that Y_{356}• equilibrated with F_2Y_{731}• or F_2Y_{730}•.[14] The analysis was facilitated by the unique F_2Y• features arising from ^{19}F and ^1H-β hyperfine interactions that are observed in both the low- and high-field regions of the EPR spectrum.[11,13] This spectroscopic handle gave us the first opportunity to investigate the effect of the protein environment on the reduction potentials of the pathway Y•'s. Quantitation of Y_{356}• in $\beta2$ and F_2Y_{731}• (or F_2Y_{730}•) in $\alpha2$ by EPR spectroscopy allowed estimation of a $\Delta E^{\circ\prime}(Y_{731/730}-Y_{356})$ of ~100 mV.[14] The thermodynamic landscape of the RT pathway constructed from these studies is shown in Figure 1. We proposed that the overall

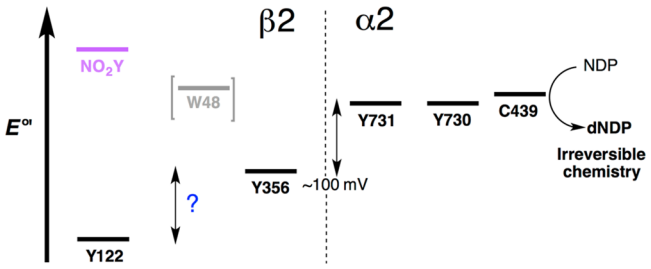

Figure 1. Proposed thermodynamic landscape of the PCET pathway at 25 °C and pH 7.6. The overall reaction is proposed to be thermodynamically uphill and driven forward by the rapid irreversible loss of water from NDP substrate in the active site of $\alpha2$. No direct evidence is available for the presence of a discrete W_{48} radical intermediate. Studies performed on NO_2Y_{122}•-$\beta2$ determined the relative reduction potentials of Y_{356}, Y_{731}, and Y_{730}.

RT pathway in wt RNR is thermodynamically uphill and driven forward by the nucleotide reduction process, specifically the rapid irreversible cleavage of the C2−OH bond[18] of the substrate and loss of water (10^6–10^9 s^{-1})[19−21] in the active site of $\alpha2$. Equilibration of the pathway Y's could be measured because oxidation of Y_{356} by NO_2Y_{122}• is irreversible. Unfortunately, this same feature prohibited use of NO_2Y_{122}•-$\beta2$ to monitor equilibration of NO_2Y_{122}• and Y_{356}•.

To obtain insight over the entire thermodynamic landscape of RNR, $\Delta E^{\circ\prime}(Y_{122}-Y_{356})$ must be defined. A recently engineered $\beta2$ containing 2,3,5-trifluorotyrosine (F_3Y) at position 122 provides an avenue to assess the $\Delta E^{\circ\prime}(Y_{122}-Y_{356})$ energetics.[13,22] The reaction of F_3Y_{122}•-$\beta2$, $\alpha2$, CDP, and ATP results in rapid formation of dCDP concomitant with accumulation of Y_{356}• (20–30 s^{-1}). In contrast to NO_2Y_{122}•-$\beta2$, however, we have demonstrated that Y_{356}• can reoxidize F_3Y_{122} and that this reoxidation process is rate-limiting for subsequent turnovers.[22] The reversible nature of Y_{356} oxidation in F_3Y_{122}•-$\beta2$ has led to the studies described herein and provided the opportunity to investigate the relative reduction potentials of F_3Y_{122}• and Y_{356}•.

In this work, we report the temperature (2–37 °C) and pH-dependent (6.8–8.0) quantitation of F_3Y_{122}• and Y_{356}• in the reaction of F_3Y_{122}•-$\beta2$, Y_{731}F-$\alpha2$ (or Y_{730}F-$\alpha2$), CDP, and ATP by EPR spectroscopy. At pH 7.6 and 25 °C, $\Delta E^{\circ\prime}(F_3Y_{122}\bullet-Y_{356}\bullet)$ values of 20 ± 10 and 5 ± 7 mV are observed in the reactions with Y_{731}F-$\alpha2$ and Y_{730}F-$\alpha2$, respectively. The ability to equilibrate F_3Y_{122}• and Y_{356}• with Y_{731}F-$\alpha2$ also provided the opportunity to investigate the fate of the Y_{356} proton upon oxidation of this pathway Y. A plot of the $\log([Y_{356}\bullet]/[F_3Y_{122}\bullet])$ versus pH provides a slope of 1.2 ± 0.2 at 25 °C, consistent with rapid release of the Y_{356} proton to solvent. With a knowledge of the pH dependence of the $F_3Y_{122}\bullet/Y_{356}\bullet$ equilibration, we have implemented an experimental design to determine the thermodynamic difference between Y_{122} and Y_{356}. Increasing amounts of Y_{356}• are observed with increasing pH. Additionally, by choosing an appropriate pH the reduction potential of F_2Y can be tuned to be essentially equal to that of Y,[23−25] but oxidized F_2Y• has the potential to be spectroscopically observable because of the ^{19}F hyperfine features.[13] Thus, the ability of Y_{122}• to oxidize F_2Y incorporated in place of Y_{356} (F_2Y_{356}-$\beta2$) was tested. Rapid freeze-quench (RFQ)-EPR spectroscopy of the reaction between F_2Y_{356}-$\beta2$, Y_{731}F-$\alpha2$, CDP, and ATP at pH 8.2 and 25 °C revealed F_2Y_{356}• at 3 ± 1% of the total radical concentration. This observation provided a $\Delta E^{\circ\prime}(F_2Y_{356}\bullet-Y_{122}\bullet)$ of 70 ± 5 mV, which along with our recent measurement of the reduction potential of F_2Y in a protein environment[23,25] gives an estimate of $\Delta E^{\circ\prime}(Y_{356}\bullet-Y_{122}\bullet)$ of ~100 mV at pH 7.6. The results of the site specifically incorporated unnatural amino acids described herein together with our previous studies allow us to propose a thermodynamic landscape for the RT pathway in the *E. coli* class Ia RNR that is ~200 meV uphill between Y_{122} and C_{439}.

MATERIALS AND METHODS

Materials. $(His)_6$-Y_{731}F-$\alpha2$,[26] $(His)_6$-Y_{730}F-$\alpha2$,[26] wt-$\alpha2$ (specific activity of 2500 nmol/min/mg),[26] tyrosine phenol lyase,[27] F_2Y,[28] and F_3Y[28] were isolated; apo F_3Y_{122}-$\beta2$ was expressed, isolated, and reconstituted[22] as previously reported. F_2Y_{356}-$\beta2$ (0.7 Y•/$\beta2$) was available from an earlier study.[29] CDP and ATP were purchased from Sigma-Aldrich. Assay buffer consists of 50 mM HEPES pH 7.6, 15 mM $MgSO_4$, and 1 mM EDTA unless otherwise specified. In all studies, the temperature was controlled using a Lauda RM6 circulating water bath. The reference spectrum for F_3Y_{122}• and its simulation were recently reported.[30] The reference spectrum for Y_{356}•, which was obtained as the signal averaged sum of the Y_{356}• difference spectra, is in agreement with the previously reported spectrum.[17]

Hand-Quench EPR Analysis of Y_{356}• Formation as a Function of Temperature. Assay mixtures containing a final volume of 250 μL with 25 μM Y_{731}F-$\alpha2$, 1 mM CDP, and 3 mM ATP in assay buffer were incubated in a water bath set between 2 and 37 °C. F_3Y_{122}•-$\beta2$ (0.8 $F_3Y\bullet/\beta2$) was added to a final concentration of 25 μM to initiate each of the reactions. The reaction mixtures were then transferred to X-band EPR tubes maintained in the water bath, and the samples were frozen in liquid isopentane (−140 °C) at 20 s (or 1 min) and analyzed by X-band EPR spectroscopy The EPR parameters were as follows: microwave frequency 9.45 GHz; power 30 μW; modulation amplitude 1.50 G; modulation frequency 100 kHz; time constant 40.96 ms; and conversion time 20.48 ms. Three independent sets of experiments were carried out.

Analysis of EPR Data. Two different methods, A and B, were used for quantitation of the two radicals due to the small changes in the EPR spectra associated with the changes in T and pH (section described subsequently), the complexity of the spectra, and the half-sites reactivity of RNR (that is, 50% of the starting $F_3Y\bullet/\beta2$ remains unchanged). The data shown in the Results section were analyzed by method A, chosen for visualization purposes. Both methods of analysis provide similar outcomes and are summarized in Tables S1 and S2. The total spin remained unchanged in all the samples throughout the analyses. The $\Delta E^{\circ\prime}(F_3Y_{122}\bullet-Y_{356}\bullet)$ was calculated based on the two quantitation methods described below and using

$$\Delta E^{\circ\prime} = \frac{RT \ln K_{eq}}{F} \quad (1)$$

DOI: 10.1021/jacs.6b08200
J. Am. Chem. Soc. 2016, 138, 13706−13716

where $K_{eq} = [Y_{356}\bullet]/[F_3Y_{122}\bullet]$, R is the ideal gas constant, T is the temperature (K), and F is Faraday's constant.

Method A: Quantitation of $F_3Y_{122}\bullet$ and $Y_{356}\bullet$ in β2 as a Function of Temperature. Each EPR spectrum was normalized to have the same intensity in the low-field features associated with $F_3Y_{122}\bullet$. In this representation of the spectra, the intensity of $F_3Y_{122}\bullet$ remains constant, allowing easier visualization of the $Y_{356}\bullet$ signal that grows in with increasing temperature. Using the low-field features in the spectrum of $F_3Y_{122}\bullet$, $F_3Y_{122}\bullet$ was subtracted from each composite spectrum. The amount of $Y_{356}\bullet$ remaining was determined by double integration.[13] The $Y_{356}\bullet$ spectrum observed for each sample was identical by this method.

Method B. A detailed description of data analysis by method B is presented in the Supporting Information. In the first step, the baseline was removed from each spectrum with a second-order polynomial fit. In the second step, the 50% signal from $F_3Y_{122}\bullet$ that remains in the composite spectra due to half sites reactivity was subtracted using the $F_3Y_{122}\bullet$-β2 reference spectrum (Figure S1A). The resulting composite spectra show the interconversion between $F_3Y_{122}\bullet$ and $Y_{356}\bullet$ as a function of temperature (Figure S1B), free from the complications caused by half sites reactivity. However, this subtraction increases the noise level of the spectra, so the relative amounts of $F_3Y_{122}\bullet$ and $Y_{356}\bullet$ cannot be determined reliably by eye. Therefore, a script was written in Matlab 2016a to automatically subtract out the remaining $F_3Y_{122}\bullet$. The amount of remaining $F_3Y_{122}\bullet$ was determined by adjusting the intensity of the $F_3Y_{122}\bullet$-β2 reference spectrum (Figure S1C) until the least-squares difference between the reference spectrum and the composite spectra in the g-value interval between 2.0363 and 2.0390 (this defines the highest S/N region of the low-field $F_3Y_{122}\bullet$ features) was minimized. The amount of $Y_{356}\bullet$ after subtracting out the remaining $F_3Y_{122}\bullet$ was determined by double integration. The $Y_{356}\bullet$ spectrum determined by this method was the same in each sample (Figures S1D and S2).

Temperature-Dependent Equilibration of $F_3Y_{122}\bullet$ and $Y_{356}\bullet$ within the Same Sample. To support equilibration between $F_3Y_{122}\bullet$ and $Y_{356}\bullet$ in β2 (at 25 °C) as described above in the Y_{731}F- and Y_{730}F-α2 reactions, the EPR spectrum of the 20 s sample was first recorded. Each sample was then thawed by submersion into a room-temperature water bath and was then incubated in a 2 °C water bath for 15 s followed by refreezing and reacquisition of the EPR spectra. The samples were thawed again and then placed in a 25 °C water bath for 15 s, refrozen, and the EPR spectrum rerecorded. Quantitation of $Y_{356}\bullet$ and $F_3Y_{122}\bullet$ was performed as described above.

RFQ-EPR Analysis of $Y_{356}\bullet$ Formation as a Function of Temperature. RFQ experiments were performed on an Update Instruments 1019 syringe ram unit and a model 715 syringe ram controller (ram speed 1.25 cm/s). $F_3Y_{122}\bullet$-β2 (70 μM, 0.8 $F_3Y\bullet/\beta2$) and CDP (2 mM) in assay buffer in one syringe were mixed with Y_{731}F-α2 (70 μM) and ATP (6 mM) in a second syringe and incubated at varying temperatures (2−37 °C) for either 4 or 10 s. The reaction mixture was then sprayed into liquid isopentane,[31] and the crystals were packed into EPR tubes for analysis by X-band EPR spectroscopy. A packing factor of 0.60 ± 0.02 was calculated for $F_3Y_{122}\bullet$-β2. Data acquisition and analysis were performed as described for the hand-quench (HQ) method.

HQ-EPR Analysis of $Y_{356}\bullet$ Formation as a Function of pH. Y_{731}F-α2 (25 μM), $F_3Y_{122}\bullet$-β2 (25 μM, 0.6−0.8 $F_3Y\bullet/\beta2$), CDP (1 mM), and ATP (3 mM) were combined in 50 mM MES (pH 6.8) or HEPES (pH 7.0−8.0), 15 mM $MgSO_4$, and 1 mM EDTA and incubated at 5 or 25 °C. Reaction mixtures were transferred to X-band EPR tubes also maintained in the water bath and frozen in liquid isopentane (−140 °C) within 20 s (or 1 min) for analysis by X-band EPR spectroscopy using methods A and B described above. The data were fit to

$$\log K = \mathrm{pH} - \mathrm{p}K_a \qquad (2)$$

where $K = [Y_{356}\bullet]/[F_3Y_{122}\bullet]$.

RFQ-EPR Analysis of the Reaction of F_2Y_{356}-β2, Y_{731}F-α2, CDP, and ATP. Y_{731}F-α2 (80 μM) and 6 mM ATP in 50 mM TAPS pH 8.2, 15 mM $MgSO_4$, and 1 mM EDTA in one syringe was rapidly mixed at 25 °C with an equal volume of F_2Y_{356}-β2 (80 μM, 0.7 $Y\bullet/\beta2$) and CDP (2 mM) in the same buffer in the second syringe. The reaction was aged for 10, 20, or 40 s, quenched in liquid isopentane, and analyzed by X-band EPR spectroscopy as described above. The EPR parameters were as follows: microwave frequency 9.45 GHz; power 30 μW; modulation amplitude 1.50 G; modulation frequency 100 kHz; time constant 163.8 ms; and conversion time 20.48 ms. The total number of scans were 700 (10 s sample), 600 (20 s sample), and 560 (40 s sample). The simulations were carried out using EasySpin v5.0.18[32] in Matlab R2015b. The g-values (2.0073, 2.0044, and 2.0022) and β-^{1}H hyperfine tensor (54, 52, and 54 MHz) were fixed in the simulations using previously reported values for $Y_{356}\bullet$ in the reaction of $NO_2Y_{122}\bullet$-β2 with Y_{731}F-α2[14] and the ^{19}F and β-^{1}H hyperfine values of $F_2Y_{122}\bullet$.[30]

RESULTS

Temperature-Dependent Distribution of $F_3Y_{122}\bullet$ and $Y_{356}\bullet$ in β2 in the Presence of CDP, ATP, and Y_{731}F-α2 (or Y_{730}F-α2). We have recently shown that the reaction of $F_3Y_{122}\bullet$-β2, wt-α2, CDP, and ATP generates a kinetically and chemically competent $Y_{356}\bullet$ that can reoxidize F_3Y_{122}.[22] We hypothesized that if we carried out the same experiment with a block in the pathway (Y_{731}F-α2 or Y_{730}F-α2)[13] then equilibration of $F_3Y_{122}\bullet$ and $Y_{356}\bullet$ could be measured by EPR spectroscopy as a function of temperature, allowing determination of $\Delta E^{o\prime}(F_3Y_{122}\bullet - Y_{356}\bullet)$. $F_3Y_{122}\bullet$-β2, CDP, and ATP were incubated with Y_{731}F-α2 at varying temperatures from 2 to 37 °C for 20 s or 1 min. The samples were then frozen in liquid isopentane and examined by X-band EPR spectroscopy. Analysis of the EPR spectra at the chosen times showed no differences between the two time points, suggesting that the reaction mixture had equilibrated. The data from the 20 s incubation time is presented herein. No loss of total spin was observed between the two time points or between the different temperatures.

Interpretation of the EPR data requires consideration of the contributions of each radical and the complexities associated with *E. coli* RNR. First, Figure 2 shows a 1:1 mixture of $F_3Y_{122}\bullet$ (pink) and $Y_{356}\bullet$ (blue). The dotted vertical lines assist visualization of the features associated with $Y_{356}\bullet$ that minimally overlap with those associated with $F_3Y_{122}\bullet$. Second, reduced amounts of $F_3Y_{122}\bullet$ and $Y_{356}\bullet$ arise from unique features of the *E. coli* class Ia RNR. The amount of $F_3Y_{122}\bullet$ is typically 0.6−0.8 per β2 (instead of the theoretical 2 $F_3Y\bullet/\beta2$),

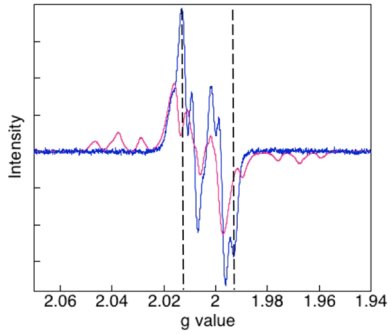

Figure 2. X-band EPR spectra of equimolar concentrations of $F_3Y_{122}\bullet$ (pink) and $Y_{356}\bullet$ (blue). All spectra presented subsequently are additive and contain the same concentration of $F_3Y_{122}\bullet$ and increasing amounts of $Y_{356}\bullet$. The dotted lines highlight the regions of the spectrum where the changes that occur upon $Y_{356}\bullet$ formation are most apparent.

DOI: 10.1021/jacs.6b08200
J. Am. Chem. Soc. 2016, 138, 13706−13716

with active $\beta 2$ containing a F_3Y_{122}• in each β monomer.[22] Furthermore, while the active form of RNR is $\alpha 2\beta 2$, the enzyme exhibits half-sites reactivity where only one of the two Y_{122}•'s (one α/β pair) is active at a time.[22] A consequence of these phenomena is the presence of 50% of the total spin as residual F_3Y_{122}• in all reaction mixtures. Thus, the data shown in Figures 3, S3, and S4 are presented using method A

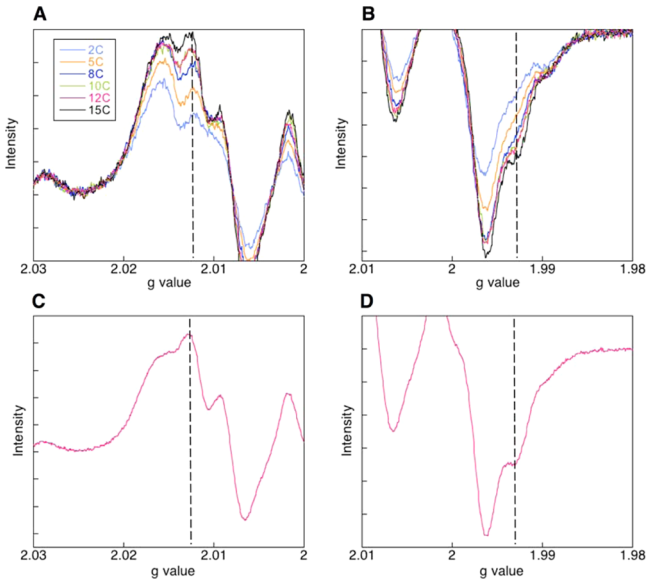

Figure 3. Composite EPR spectra of the F_3Y_{122}•-$\beta 2$/Y_{731}F-$\alpha 2$/CDP/ATP reaction as a function of temperature (2−15 °C). The composite spectrum at each temperature was acquired on three independently prepared samples. (A and B) Low- and high-field regions of the spectra for trial 1 are shown here. The color code is described in panel A. Trials 2 and 3 are shown in Figure S3. The composite EPR spectra collected between 15 and 37 °C are shown in Figure S4. (C and D) Low- and high-field regions of a simulated spectrum of a reaction mixture containing 50% each of F_3Y_{122}• and Y_{356}•. The spectrum was generated by adding the individual spectra of F_3Y_{122}• and Y_{356}• (Figure 2). The dotted lines identify spectral features that are characteristic of Y_{356}•.

described in the experimental section to allow the small changes in the amounts of Y_{356}• as a function of temperature (2, 5, 8, 10, 12, and 15 °C) to be more clearly observable. With method A, the spectra have been manipulated such that the amount of F_3Y_{122}• remains constant, while Y_{356}• grows in as a function of temperature. In this analysis method, each spectrum is normalized to have the same intensity in the low-field F_3Y_{122}• features. As shown by the dotted line in Figure 3A,B, increasing amounts of Y_{356}• can then be observed between 2 and 15 °C. Two additional replications of this experiment are shown in Figure S3. The changes in the spectra directly correlate with increasing amounts of Y_{356}• from 17 ± 5% (average of three trials at 2 °C) to 31 ± 2% (average of three trials at 15 °C) of total spin; the quantitation of these data is summarized in Table S1. In contrast with these observations, minimal changes are visualized in the composite EPR spectra recorded between 15 and 37 °C (Figure S4 and Table S1). The average amounts of Y_{356}• in the three experiments are shown in Table S1 (31 ± 2% at 15 °C and 33 ± 1% at 37 °C). The percentage Y_{356}• of total spin as a function of temperature is shown in Figure 4 (pink dots). A break in the curve is observed at ∼15 °C, and the amount of Y_{356}• does not appear to change significantly from 15 to 37 °C.

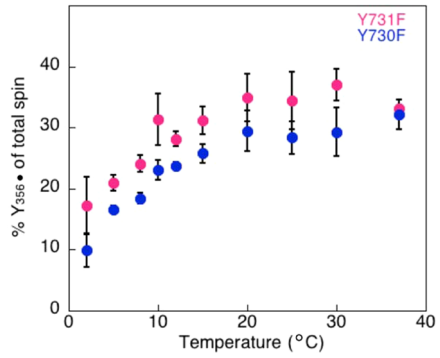

Figure 4. Temperature dependence (2−37 °C) of Y_{356}• formation in the reaction of F_3Y_{122}•-$\beta 2$, CDP, ATP, and Y_{731}F-$\alpha 2$ (pink) or Y_{730}F-$\alpha 2$ (blue). Each data point represents the average of two (blue) or three (pink) independent trials.

Control Experiments to Support F_3Y_{122}•/Y_{356}• Equilibration. Two types of experiments were carried out to provide further support for the equilibration of F_3Y_{122}• and Y_{356}•. Previous studies on adenosylcobalamin (AdoCbl) class II RNR[33] have shown that slow quenching of samples by hand shifts the equilibrium relative to rapid freezing methods. Thus, changing ratios of F_3Y_{122}• and Y_{356}• by RFQ would support equilibration of the two radical states. Preliminary experiments revealed no spin loss and minimal changes in the EPR spectra of samples quenched at 4 and 10 s using the RFQ method. The time scale for quenching was chosen based on kinetic experiments performed with F_3Y_{122}•-$\beta 2$ and wt-$\alpha 2$.[22] Thus, subsequent RFQ samples were quenched at 10 s. The results of these experiments are shown in Figure S5 and summarized in Table S1. The amount of Y• observed by RFQ is 5−10% higher than that recorded by the HQ method. However, similar trends are observed between the RFQ-EPR and HQ samples. Increasing amounts of Y_{356}• are observed between 2 and 15 °C, whereas the spectra collected between 15 and 37 °C show minimal changes in the percentage of Y_{356}• (Table S1 and Figure S6). The RFQ and HQ methods together support equilibration of F_3Y_{122}• and Y_{356}• and the ability to shift the equilibrium between the two radical states based on the quenching method.

A second experiment to support equilibration between F_3Y_{122}• and Y_{356}• was carried out as described in the Materials and Methods section. In this experiment, the EPR spectrum of a single sample that was equilibrated at 25 °C was first measured and the sample thawed, equilibrated at 2 °C, and reanalyzed by EPR spectroscopy. The sample was then thawed a final time, shifted back to 25 °C, and the EPR spectrum was recorded. The composite EPR spectra are shown in Figure S7A,B, and the amounts of Y_{356}• ascertained from these spectra are summarized in Table S3. The total spin changed minimally and the ratio of the two radicals shifted with temperature as predicted by the trend observed in Figure 4. The data together support equilibration of F_3Y_{122}• and Y_{356}• with an unusual temperature dependence.

Effect of the F Block at Residue 731 in $\alpha 2$ on the F_3Y_{122}•/Y_{356}• Equilibrium. Recent high-field (HF)-EPR spectroscopy experiments indicate that the electrostatic environment of Y_{356}• changes in a reaction containing Y_{731}F-

DOI: 10.1021/jacs.6b08200
J. Am. Chem. Soc. 2016, 138, 13706−13716

α2 relative to wt-α2.[14] Differences in reactivity between wt-α2 and Y_{731}F-α2 are also recorded for photo-RNR, which contains a [Re^{I}] photooxidant appended to the C-terminal tail of β2 (S_{355}C).[34,35] We therefore posited that the block at 731 could perturb the reduction potential of Y_{356}• compared to the wt enzyme. The equilibration experiments were repeated with Y_{730}F-α2, and as seen in Figure 4 (blue dots), variations can be observed between Y_{731}F-α2 and Y_{730}F-α2, with the former construct generating slightly higher amounts of Y_{356}•.

Calculation of $\Delta E^{\circ\prime}$(F_3Y_{122}•−Y_{356}•) from the Y_{731}F and Y_{730}F-α2 Studies. To calculate the reduction potential difference between F_3Y_{122}• and Y_{356}•, the ln K_{eq} ([Y_{356}•]/[F_3Y_{122}•]) observed in the Y_{731}F and Y_{730}F-α2 reactions at 25 °C by the HQ method were used (eq 1); $\Delta E^{\circ\prime}$(F_3Y_{122}•−Y_{356}•) at 25 °C is 20 ± 10 and 5 ± 7 mV, respectively. We note again the unusual temperature dependence of the Y_{356}• amounts with a break at 15 °C. A similar temperature dependence has been noted for steady-state dNDP formation in a 1976 study by vön Dobeln and Reichard.[36] The cause(s) of the break in Figure 4 and in the previous activity studies are unknown but are likely related to RNR conformational changes that rate-limit RT and nucleotide reduction.

Equilibration of F_3Y_{122}• and Y_{356}• as a Function of pH and Rapid Proton Exchange with Solvent during Y_{356} Oxidation. The equilibration of F_3Y_{122}• and Y_{356}• described above gave us the opportunity to investigate the fate of the proton released upon Y_{356} oxidation. Two scenarios for this proton transfer (PT) can be envisioned (Scheme 1). In one case, the proton from Y_{356} is transferred to an amino acid residue (X) and is sequestered from solvent. In the second case, the proton is in rapid exchange directly with solvent; the initial proton acceptor could be an amino acid residue (Y, Scheme 1) or a water cluster. For PT to X, the amount of Y_{356}• would be independent of pH, while for PT to Y/solvent log([Y_{356}•]/[F_3Y_{122}•]) would be directly proportional to the pH with a slope of 1. It has been previously proposed that the conserved E_{350} in β2 functions as the proton acceptor for Y_{356}.[10,37] The location of E_{350} within the C-terminal tail at the α2/β2 interface remains unknown, but its importance to catalysis has been demonstrated by site-directed mutagenesis studies.[29,37]

Scheme 1. Proposed Models for the Fate of the Y_{356} Proton

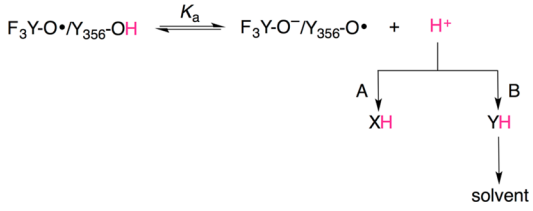

[a](A) The proton released from Y_{356} is accepted by an amino acid residue (X) and is not solvent-exchangeable. (B) The proton is in fast exchange with solvent. The initial proton acceptor (Y) is either an amino acid residue or water.

To gain insight into the PT pathway at Y_{356}, a series of studies were undertaken. F_3Y_{122}•-β2, Y_{731}F-α2, CDP, and ATP were combined in designated assay buffers (pH 6.8−8.0), incubated for 20 s or 1 min at 25 °C (or 5 °C), quenched by hand, and analyzed by EPR spectroscopy. The analysis was first carried out using method A. As with the temperature dependent studies, no variations in total spin were recorded, and no differences were observed between the spectra of samples incubated for 20 s and 1 min, observations consistent with a reaction at equilibrium. The spectral changes are shown in Figure 5A,B, and the dotted line shows an increase in the amount of Y_{356}• as the pH is increased. The composite spectra for a second trial are shown in Figure S8 (see Figure S9 for the 5 °C data), and the average amounts of Y_{356}• from the two experiments are reported in Table S2. Figure 6A shows the percentage of Y_{356}• for the pH range 6.8−8.0 at 25 °C (see Figure S10A for data from pH 6.8−7.8 for 5 °C). The percentage of Y_{356}• at pH 6.8 and 7.0 are very low (Table S2), and the percentage of Y_{356}• above pH 8.0 at 25 °C and pH 7.8 at 5 °C does not change. The maximum amounts of Y_{356}• at 25

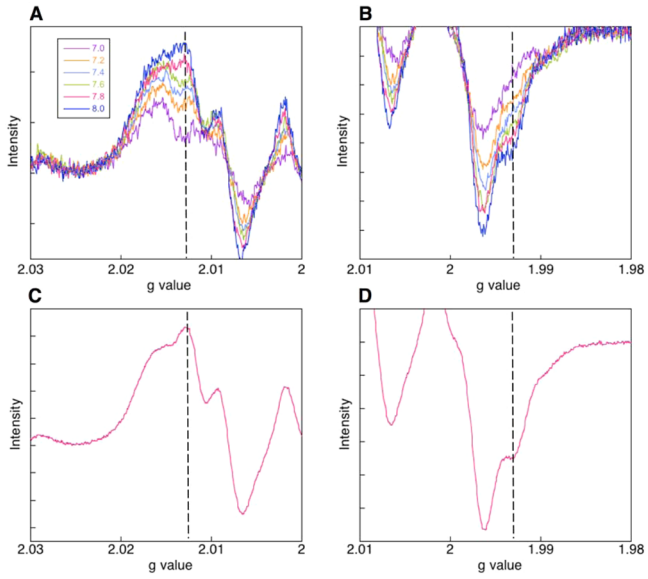

Figure 5. Composite EPR spectra of the F_3Y_{122}•-β2/Y_{731}F-α2/CDP/ATP reaction at 25 °C as a function of pH. The composite spectrum at each pH was acquired on two independently prepared samples. (A and B) The low- and high-field regions of the spectra for trial 1 are shown here. The colors represent different pH values as described in panel A. Trial 2 is shown in Figure S8. (C and D) Low- and high-field regions of a simulated spectrum of a reaction mixture containing 50% each of F_3Y_{122}• and Y_{356}•. The spectrum was generated by adding the individual spectra of F_3Y_{122}• and Y_{356}• (Figure 2). The dotted lines identify spectral features that are characteristic of Y_{356}•.

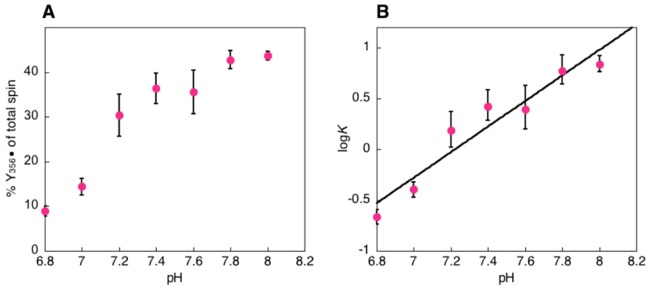

Figure 6. pH dependence of Y_{356}• formation in the reaction of F_3Y_{122}•-β2/Y_{731}F-α2/CDP/ATP at 25 °C. (A) Percentage Y_{356}• of total spin as a function of pH. (B) log K as a function of pH where K is the ratio of Y_{356}• to F_3Y_{122}•. The observed pH dependence of slope 1.2 ± 0.2 supports that the Y_{356}• proton is in fast exchange with solvent.

DOI: 10.1021/jacs.6b08200
J. Am. Chem. Soc. 2016, 138, 13706−13716

°C (43%) and 5 °C (31%) reflect the equilibrium concentrations of Y_{356}• at each temperature.

The dependence of $\log([Y_{356}\bullet]/[F_3Y_{122}\bullet])$ on pH at 25 and 5 °C are shown in Figures 6B and S10B, respectively. A slope of 1.2 ± 0.2 is measured at 25 °C (1.0 ± 0.1 at 5 °C) supporting the model in which the proton from Y_{356} is in fast exchange with solvent at both temperatures. Y_{356}• formation is favored more at 25 °C compared to 5 °C, an observation that is in accordance with our temperature-dependent distribution between the two radicals (Figure 4).

Equilibration of Y_{122}• and F_2Y_{356}• Using F_2Y_{356}-β2/α2/CDP/ATP. Although the above studies allowed establishment of $\Delta E^{\circ\prime}(F_3Y_{122}\bullet-Y_{356}\bullet)$ in F_3Y_{122}•-β2, the $\Delta E^{\circ\prime}(Y_{122}\bullet-Y_{356}\bullet)$ in wt RNR, which is essential for understanding the thermodynamics of the RT pathway, remains unknown. The pH studies described above show that maximum Y_{356}• is generated with F_3Y_{122}•-β2 at pH 8.0 or greater and 25 °C. Recent studies suggest that the difference in reduction potential between Y and F_2Y at position 356 at pH 8.2 is small (<10 mV)[25] and that the activity of F_2Y_{356}-β2 at this pH is 50% of the wt activity.[29] The pK_a of F_2Y_{356} is estimated to be 7.6 at position 356;[15] thus, at pH 8.2, >80% of F_2Y_{356} is in the deprotonated state. Due to the ability to detect small amounts of F_2Y• utilizing its unique spectroscopic features in the low- and high-field regions of the EPR spectrum, we carried out the following experiment in the hope of obtaining insight about $\Delta E^{\circ\prime}(Y_{122}\bullet-Y_{356}\bullet)$. F_2Y_{356}-β2, Y_{731}F-α2, CDP, and ATP were reacted at pH 8.2 for 10, 20, or 40 s, and the reaction was quenched using the RFQ instrument and analyzed by EPR. Quenching on the millisecond time scale was used to avoid potential shifting of the equilibrium observed with hand quenching (Table S1 and Figure S6).[33]

The RFQ-EPR data for the reaction at 20 s are shown in Figure 7, and the 10 and 40 s data are shown in Figure S11. A

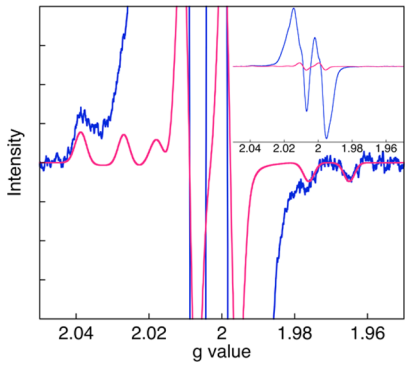

Figure 7. Reaction of F_2Y_{356}-β2, Y_{731}F-α2, CDP, and ATP monitored by RFQ-EPR spectroscopy. Expanded view of the overlay of the EPR spectrum of the reaction mixture quenched at 20 s (blue) with the simulated spectrum of F_2Y_{356}• (pink). The inset shows the full spectrum. The EPR spectra of reaction mixtures quenched at 10 and 40 s are shown in Figure S11.

view of the entire spectrum is shown in the inset in Figure 7. The results reveal small features on the low- and high-field sides that suggested the presence of F_2Y_{356}•.[13] The resolved hyperfine splittings were simulated with the "pepper" module of EasySpin as described in the Methods section. From the initial simulations, it was recognized that the β-^{1}H hyperfine parameters matched the doublet splitting on the high-field side of the spectrum, confirming the identity of this radical species as F_2Y_{356}•. The interdoublet splitting was reproduced with two equivalent ^{19}F couplings having an A_{zz} of 147 MHz.[13,30] The sharpness of the 3,5-^{19}F features are similar to those previously reported for the other pathway residues F_2Y_{122},[13] F_2Y_{731},[14] and F_2Y_{730}[14] reflecting a rigid conformation constrained by the protein environment. The A_{zz} value for F_2Y_{356}• is slightly weaker than those reported previously for the other F_2Y•'s (Table S4) and will be of importance when structural insight is obtained.

The amount of F_2Y_{356}• was similar at all three time points and was approximated from the simulated spectrum by matching the signal intensities of the wing features in the experimental and simulated spectra and comparing the double integral of the two. The greatest source of error in the analysis comes from the intrinsic line broadening factor (17 ± 4 MHz) used in all simulations.[14] The amount of F_2Y_{356}• in the 20 s sample was quantitated as 3 ± 1% of total spin. This amount of radical reflects $\Delta E^{\circ\prime}(F_2Y_{356}\bullet-Y_{122}\bullet)$ of 70 ± 5 mV, which in combination with our reduction potential studies[24,25] allows calculation of $\Delta E^{\circ\prime}(Y_{356}\bullet-Y_{122}\bullet)$ of ∼100 mV at pH 7.6 (Figure 8).

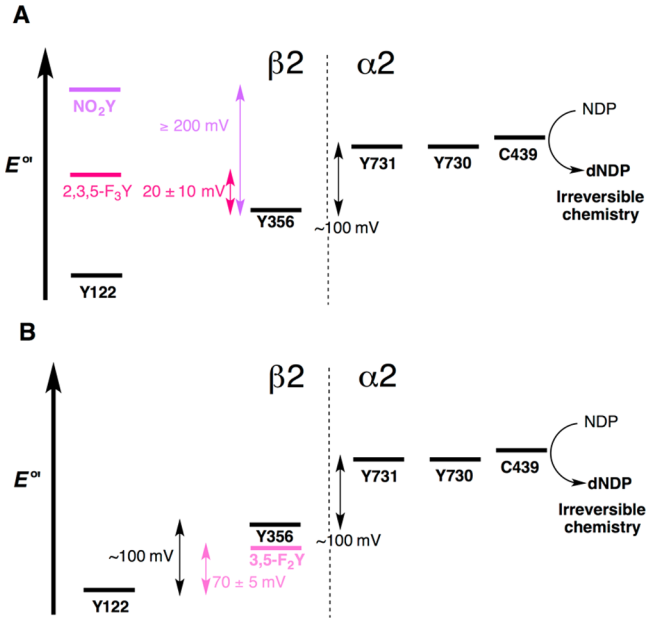

Figure 8. Current thermodynamic landscape of the PCET pathway at 25 °C and pH 7.6. (A) Studies performed on F_3Y_{122}•-β2 described in this work provided an estimate of the relative reduction potentials of F_3Y_{122} and Y_{356}. (B) Studies performed on F_2Y_{356}-β2 provided an estimate of the relative reduction potentials of Y_{122} and Y_{356}. W_{48} has been removed from the landscapes for the sake of clarity.

DISCUSSION

RNRs are divided into three classes based on the metallocofactor used for thiyl radical formation.[6] All classes of RNR initiate nucleotide reduction by thiyl radical mediated 3′-H atom abstraction from the substrate.[18] The reducing equivalents for the reaction are provided by oxidation of a pair of cysteines in the active site,[38−40] with a subtype of the class III enzyme which uses formate as the reductant as the sole exception.[41] The class II RNR utilizes adenosylcobalamin as a cofactor,[3] whereas the class III system uses a stable glycyl radical to generate the transient thiyl radical.[42] These

DOI: 10.1021/jacs.6b08200
J. Am. Chem. Soc. 2016, 138, 13706−13716

observations raise the issue of why and how a 35 Å oxidation process evolved in the class I RNR[9] instead of a direct H atom abstraction process that is used by the other classes.[18] The turnover number for deoxynucleotide formation (2−10 s^{-1})[43] and the large distance between Y_{122}• and C_{439} in the class Ia RNR[9,44] require intermediates in the oxidation process and raise the question of how the thermodynamic and kinetic landscape of this process has evolved to maintain balanced dNTP pools and avoid self-inactivation. Investigation of this oxidation process has proven challenging primarily due to the slow rate-limiting conformation changes that occur in the $\alpha 2\beta 2$ complex subsequent to S/E binding and prior to RT.[43] Furthermore, the substantial overlap of the EPR spectra of Y•'s would make identification of these species challenging even if the rate-limiting step could be altered.

Thermodynamic Landscape of the RT Pathway within the β2 Subunit. Recently we have assembled the diferric-NO_2Y_{122}• cofactor ($t_{1/2}$ of 40 s at 25 °C) in the β2 subunit of RNR. NO_2Y• is ∼200 mV more oxidizing than Y•[16] and has provided insight about the thermodynamic landscape for the RT pathway in two ways. When NO_2Y was substituted in place of each Y_x in the pathway (Figure 1, where x = 122 and 356 in β2 and 731 and 730 in α2), the resulting mutants were all catalytically inactive.[15] Thus, perturbation of the reduction potential by +200 mV is sufficient to shut down the RT pathway. This observation supports previous proposals about the extent to which uphill steps can be accommodated in electron transfer (ET) pathways in general,[45,46] and in RNR specifically.[46,47] NO_2Y substitution at each position also allowed assessment of the protein environment perturbation of the pK_a of the phenol, relative to the pK_a in solution. Positions 356, 731, and 730 were found to be minimally perturbed (+0.4, 1.0, and 1.2 units) and position 122 was found to be greatly perturbed (greater than +3 units).[15] We assume that a similar position-dependent perturbation occurs with the F_nY's incorporated at 356, 731, and 730. However, given the unique environment of Y_{122} (hydrophobic and adjacent to the diferric cluster), this assumption cannot be made.

The ability to generate NO_2Y_{122}• in β2 allowed observation of the equilibration of the pathway tyrosyl radicals: Y_{356}•, F_2Y_{731}•, or F_2Y_{730}•. This observation was fortuitous as the equilibration arose from several unanticipated consequences of NO_2Y_{122}• substitution. First, this mutant uncoupled the conformational gating masking the wt RT process. DeoxyCDP and Y_{356}• formed during reverse RT occurred at 100−300 s^{-1},[17] much faster than the wt turnover of 5 s^{-1}.[43] Although Y_{356}• was generated rapidly, it was unable to reoxidize the NO_2Y^- phenolate formed during forward RT (Scheme 2). Thus, a block in the pathway occurred without additional mutations. We note that in wt RNR there is evidence to suggest that a proton is delivered to Y_{122}• from the water on Fe1 in the cluster during forward RT (Scheme 2).[48] In the case of NO_2Y, this does not occur, and the phenolate is formed. It is likely that the water on Fe1 remains protonated providing insight into the relative pK_as of Y_{122} and Fe1−H_2O. Since the NO_2Y phenol has a pK_a of 7.1, this raises issues about the protonation state of F_3Y_{122}• (pK_a of phenol is 6.4) on reduction during forward RT (Scheme 2).

Due to the inability to investigate equilibration of Y_{356}• with Y_{731}• and Y_{730}• in wt RNR, F_2Y was inserted in place of either Y_{731} or Y_{730}, providing access to the unique EPR spectroscopic features of F_2Y•.[14] These experiments showed the presence of 10−15% F_2Y_{731}• (or F_2Y_{730}•). A knowledge of the pK_a perturbation of ∼1 unit at these positions[15] in conjunction with differential pulse voltammetry (DPV) studies on the N-acetyl-3,5-difluoro-L-tyrosinamide[24] provided an estimate of 85−95 mV for the reduction potential difference between Y_{731}• (or Y_{730}•) and Y_{356}•. This calculation agreed with the results from a second experiment where NO_2Y_{122}•-β2 was reacted with [β-$^2H_2$]Y-α2 and probed for variations in the EPR spectrum. Temperature dependent studies provided the $\Delta E^{\circ\prime}$([β-$^2H_2$]Y•−Y_{356}•) of ∼100 mV (Figures 1 and 8). These studies together showed that the RNR protein environment perturbs F_2Y and Y in a similar fashion and that F_2Y is a good probe for the reduction potential of both Y_{731} and Y_{730}.

More recently, we have reported the detailed kinetic analysis of the F_3Y_{122}•-β2/α2/CDP/ATP reaction.[22] This reaction generates a kinetically and chemically competent Y_{356}• at 20−30 s^{-1}, which in contrast to Y_{356}• generated by NO_2Y_{122}•-β2 is capable of reoxidizing F_3Y_{122}. The reoxidation process is conformationally gated and rate-limiting for subsequent dCDP formation and only observed after several turnovers upon exhaustion of the reducing equivalents. The observation of both radicals (F_3Y_{122}• and Y_{356}•) and activity required that we utilize a pathway block in order to monitor equilibration. $Y_{731}F$-α2 ($Y_{730}F$-α2) served that purpose as our previous studies showed that these mutants still allow Y_{356}• generation.[13]

To quantitate the reduction potential increase that occurs upon replacement of Y_{122} with F_3Y_{122}, it is important to determine whether the latter is reduced to the phenol or phenolate (F_3Y_{122} vs $F_3Y_{122}^-$) during RT (Scheme 2). We favor the model where $F_3Y_{122}^-$ is generated upon RT. In support of this proposal is the observation of $NO_2Y_{122}^-$ in the NO_2Y_{122}•-β2 experiments.[17] The solution pK_a of NO_2Y is 7.1,[16] and the visualization of $NO_2Y_{122}^-$ can be rationalized if Fe1−H_2O has a pK_a between 8.0 and 10.0. Although ferric iron typically reduces the pK_a of bound water,[49] di-iron clusters have been known to shift this value into the physiological pH range (pH > 7.0)[50] in a protein-environment-dependent manner. The diferric cluster environment in the class Ia RNR is unique and as noted above perturbs the pK_a of Y_{122} by >3 units.[15] If the pK_a of Fe1−H_2O is perturbed to >8.0, then initiation of the reaction with F_3Y_{122}• would primarily result in the generation of $F_3Y_{122}^-$. The

Scheme 2. First PCET Step in the RT Pathway of *E. coli* Class Ia RNR

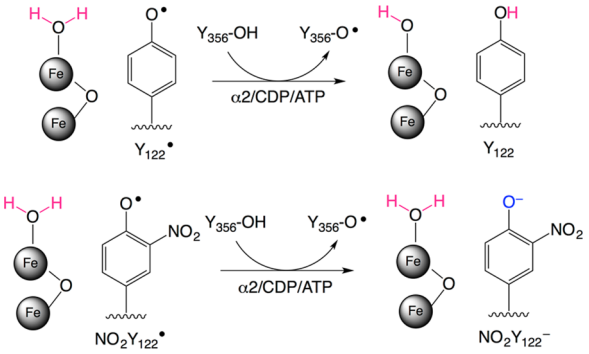

[a](A) In the wt-β2/α2/CDP/ATP complex, PT from Fe1−H_2O to Y_{122}• occurs concomitant with ET from Y_{356} to Y_{122}•. (B) In the NO_2Y_{122}•-β2/α2/CDP/ATP complex, ET from Y_{356} to Y_{122}• generates the NO_2Y^- phenolate. RT initiation in F_3Y_{122}•-β2 is proposed to generate the $F_3Y_{122}^-$ phenolate (Scheme 1).

DOI: 10.1021/jacs.6b08200
J. Am. Chem. Soc. 2016, 138, 13706−13716

protonation state of F_3Y_{122}, while favored to be deprotonated, is unknown and is under investigation.

The potential difference of ~20 mV calculated between F_3Y_{122}• and Y_{356}• (Figure 4) makes generation of $F_3Y_{122}^-$ an appealing model. We predict that $\Delta E^{\circ\prime}(NO_2Y_{122}\bullet/NO_2Y_{122}^- - Y_{356}\bullet/Y_{356})$ is ≥200 mV, owing to the inability of Y_{356}• to reoxidize NO_2Y^-. With these two values, we can estimate $\Delta E^{\circ\prime}(NO_2Y_{122}\bullet/NO_2Y_{122}^- - F_3Y_{122}\bullet/F_3Y_{122}^-)$ as greater than or equal to ~184 mV. This calculation agrees with the predicted potential difference between these two analogs based on the solution DPV data collected on the protected amino acids (~180 mV).[24] Unfortunately, we cannot at present directly extrapolate the potential difference calculated between $NO_2Y_{122}\bullet/NO_2Y_{122}^-$ (or $F_3Y_{122}\bullet/F_3Y_{122}^-$) and $Y_{356}\bullet/Y_{356}$ to $Y_{122}\bullet/Y_{122}$. This is primarily due to the unique nature of residue 122's environment compared to that of the other pathway Y's. The Y_{122} site is not in equilibrium with solvent[48] over the time course of our experiments (<20 s); its reduction potential is pH-independent and is directly determined by the dielectric constant of the protein environment. Due to these reasons, we turned our attention to an alternate way to monitor equilibration of Y_{122}• and Y_{356}• where the native Y_{122}• remains intact but Y_{356} is replaced with F_2Y_{356}.

Our observations with NO_2Y_{122}•-β2[14] and the pH-dependent studies reported herein suggest that $\Delta E^{\circ\prime}(Y_{122}\bullet/Y_{122} - Y_{356}\bullet/Y_{356})$ can be easily extrapolated from $\Delta E^{\circ\prime}(Y_{122}\bullet/Y_{122} - F_2Y_{356}\bullet/F_2Y_{356}^-)$. The proton from F_2Y_{356} is in rapid exchange with solvent (Figures 6B and S10B), and at an appropriate pH, we predict that its reduction potential is a good approximation of Y_{356}. The reaction of F_2Y_{356}-β2/Y_{731}F-α2/CDP/ATP was carried out at pH 8.2 to maximize the chances of observing the F_2Y_{356}• signal and revealed similar amounts of F_2Y_{356}• at 10, 20, and 40 s, supporting equilibration. The observed percentage of F_2Y_{356}• (3%) provides an estimation of $\Delta E^{\circ\prime}(F_2Y_{356}\bullet/F_2Y_{356}^- - Y_{122}\bullet/Y_{122})$ of ~70 mV. At pH 8.2, the reduction potentials of the $F_2Y_{356}\bullet/F_2Y_{356}^-$ and $Y_{356}\bullet/Y_{356}$ couples are predicted to be roughly the same.[24,25] At pH 7.6, the standard assay conditions, the reduction potential of Y_{356} is expected to increase by ~30 mV,[24,25,51] providing a $\Delta E^{\circ\prime}(Y_{356}\bullet - Y_{122}\bullet)$ of ~100 mV (Figure 8B). Finally, we note that our data taken together propose that at 25 °C and pH 7.6 F_3Y_{122} is ~120 mV more oxidizing than Y_{122} within the RNR protein environment. This difference is 10 times greater than we had originally predicted based on the solution DPV data collected on the N-acetyl-fluoro-L-tyrosinamide derivatives.[11] We note that this original prediction assumed that both F_3Y• and Y• are reduced to the corresponding phenols during turnover.

Relationship between the Thermodynamic Landscape and Kinetics. It is important to note that the equilibration studies described in this work were performed under nonturnover conditions (with Y_{731}F-α2 or Y_{730}F-α2). Thus, a key issue to address is whether the protein environment can alter the thermodynamic landscape to lower $\Delta E^{\circ\prime}(Y_{356}\bullet - Y_{122}\bullet)$ and facilitate turnover. Although this is a likely possibility, we argue that oxidation of Y_{356} by Y_{122}• must be uphill even under turnover conditions. Evidence for this conclusion is provided by our combined studies with wt RNR,[43] F_3Y_{122}•-β2,[22] and NO_2Y_{122}•-β2.[17]

In the case of wt RNR, investigation of RT has been hindered by the inability to monitor Y_{122}• disappearance and reappearance during turnover.[43] To account for this observation, we have previously modeled that the reverse RT process in wt RNR in which Y_{356}• reoxidizes Y_{122} must be downhill and rapid (10^3 s^{-1}).[43] In the case of F_3Y_{122}•-β2, we have measured formation of Y_{356}• (20−30 s^{-1}) and demonstrated that reoxidation of F_3Y_{122} by Y_{356}• is slow (0.4−1.7 s^{-1}) and rate-limiting for multiple turnovers.[22] In the NO_2Y_{122}•-β2 system, Y_{356}• accumulates (100−300 s^{-1}) due to the inability of this pathway radical to reoxidize NO_2Y^- subsequent to the first turnover.[17] Taken together, these studies suggest that Y_{356}• can be observed during turnover only when reverse RT is slowed down (F_3Y_{122}•-β2) or completely inhibited (NO_2Y_{122}•-β2) and is partly a result of the potential difference between Y_{122} and Y_{356}. DPV studies have estimated that reduction potential increases in the order Y < F_3Y < NO_2Y.[16,24] In accordance with this prediction, the rate constant for forward RT that generates Y_{356}• increases with increasing driving force, whereas the rate constant for reverse RT decreases with driving force, reinforcing our model that oxidation of Y_{356} by the native Y_{122}• is uphill. We have previously proposed that the conformational change that triggers RT targets the initial PT step from Fe1−H_2O to Y_{122}• (Scheme 2).[48] Uncoupled PT and ET in NO_2Y_{122}•-β2, and potentially F_3Y_{122}•-β2, suggest that we may have overcome this conformational gating and obtained direct insight into the thermodynamic effect of replacing Y_{122} with these unnatural analogs. Further support for this model is obtained when the forward RT rate constants in NO_2Y_{122}•-β2 and F_3Y_{122}•-β2 are predicted using the Moser−Dutton equation[52] (eq 3) for dependence of k_{ET} on distance (R) and driving force (ΔG).

$$\log k_{ET} = 15 - 0.6R - 3.1(\Delta G + \lambda)^2/\lambda \quad (3)$$

Assuming identical distances and reorganizational energies (λ) for ET in NO_2Y_{122}•-β2 and F_3Y_{122}•-β2, the individual expressions for log k_{ET} can be combined to assess the effect of the driving force differences (ΔG, 200 mV vs 20 mV, Figure 8A) on k_{ET}. The net equation requires an estimation of λ; by varying the reorganizational energy from 0.7 to 1.4 eV,[45] k_{ET} in NO_2Y_{122}•-β2 was calculated to be 9- to 11-fold faster than k_{ET} in F_3Y_{122}•-β2. This approximation is similar to our experimental data (5- to 15-fold) supporting the idea that the driving force dictates the kinetics in these mutant RNRs and further that both NO_2Y_{122}• and F_3Y_{122}• are reduced to the corresponding phenolates during RT.

Based on our static thermodynamic picture constructed from the studies with NO_2Y_{122}•-β2 and those reported herein, we propose that the landscape from Y_{122} to Y_{730} is ~200 meV uphill (at 25 °C and pH 7.6, Figure 8B). The landscape between Y_{730} and 3′ hydrogen atom abstraction from the nucleotide must further be taken into account to make deoxynucleotides. Electrochemical measurements on the cysteine within glutathione and Y have revealed similar midpoint potentials at pH 7.0,[53] providing an estimation of ~0.04% C_{439}• formation in the $\alpha2\beta2$ complex. Given the predicted rate constant for H_2O loss from the 2′ position (10^6−10^8 s^{-1})[19−21] of the nucleotide, the rate of this reaction using 0.04% C_{439}• would be ~10^2- to 10^4-fold faster than conformationally gated nucleotide reduction (2−10 s^{-1}).[43]

The above calculation assumes that the reaction landscape is isoenergetic subsequent to generation of Y_{731}•. However, DFT calculations performed on the individual crystal structure of α2 and on model systems have provided an estimate of ~120 mV for $\Delta E^{\circ\prime}(C_{439}\bullet - Y_{730}\bullet)$[54,55] and ~90−260 mV for 3′ H atom abstraction by C_{439}•.[6,56−58] If the measured $\Delta E^{\circ\prime}(Y_{730}\bullet - Y_{122}\bullet)$ of 200 mV is reflective of the thermodynamic landscape under turnover conditions, then we estimate that the combined

DOI: 10.1021/jacs.6b08200
J. Am. Chem. Soc. 2016, 138, 13706−13716

steps of C_{439} oxidation and 3′ H atom abstraction must be <200 meV uphill to maintain a turnover number of >10 s^{-1}.

The DFT calculations were based on a structure of α2 alone with poor electron density for the substrate and in the absence of allosteric effector. It is likely that the RT pathway and the active site in α2 will be conformationally altered in the active α2/β2/S/E complex. Furthermore, uphill reactions can be partially compensated for by decreasing the ET distance between donor and acceptor[45,46] and in the case of PCET reactions by controlling the positioning of the proton acceptor. The distances between Y_{122}, Y_{356}, and Y_{731} remain unknown because of the disordered C-terminal tail of β2. Thus, structures of the α2β2 subunit interface and knowledge of how these structures are altered in the presence of S and E binding to α2 are crucial to understanding the overall landscape of the reaction and the tuning of the individual steps in the RT process. Nonetheless, we believe from the studies described herein, that the overall reaction from Y_{122}• reduction to 3′-hydrogen atom abstraction of NDP is uphill and driven forward by rapid and irreversible loss of H_2O from the NDP (Figure 8).[19−21]

PCET across the β/α Interface Involves Fast Proton Exchange between Y_{356} and Solvent. The equilibrium between F_3Y_{122}• and Y_{356}• as a function of pH has further provided important insight about the fate of the Y_{356} proton upon its oxidation. It was originally proposed that a specific sequestered amino acid residue within β2 functioned as the proton acceptor.[10] However, the slope of 1 associated with a plot of log([Y_{356}•][F_3Y_{122}•]) versus pH (Figure 6B) is consistent with the rapid exchange of the Y_{356} proton with solvent at the subunit interface either through an amino acid residue or a water cluster functioning as the initial proton acceptor (Scheme 1). Three distinct types of experiments are currently the basis for favoring the latter possibility.[29,35,37,59,60]

The most compelling support for this model has been the work of Bennati and co-workers using multifrequency EPR and [^{2}H]-electron−nuclear double resonance (ENDOR) spectroscopic methods on mutant RNRs containing the radical trap, 3-aminotyrosine (NH_2Y). This unnatural amino acid has site specifically replaced Y_{356}, Y_{731}, or Y_{730}, leading to accumulation of NH_2Y• in each case upon incubation with the second subunit, S, and E.[26,61] HF-EPR studies on NH_2Y•'s,[55,59] specifically the g_x component of their g tensors, revealed that the electrostatic environment of all three NH_2Y•'s are perturbed, but that of NH_2Y_{356}• is perturbed to a greater extent than either NH_2Y_{731}• or NH_2Y_{730}•. In contrast with NH_2Y_{731}• or NH_2Y_{730}•, no moderate hydrogen bonding interactions were observed with NH_2Y_{356}• by HF-[^{2}H] ENDOR spectroscopy.[59] The studies together led to the proposed importance of water clusters in proton removal at the subunit interface.[59]

Using a very different approach, recent studies have been carried out with photo-RNRs in which a photooxidant is attached site specifically to residue 355 in β2 and F_nY (n = 2 or 3) or W replaces Y_{356}. In the presence of α2, S, and E and with light initiation, these constructs exert significant control in facilitating PT during oxidation of residue 356, shuttling reactive intermediates between the subunits and in the case of W, rapid PT out of the α/β interface.[35,60]

Finally, prior to the studies reported herein, the conserved residue E_{350} located on the flexible C-terminal tail of β2 near Y_{356} in sequence space, was considered to be the most likely amino acid candidate that could function as a proton acceptor for Y_{356}. Mutation of E_{350} to A abolished RNR activity,[37] an observation we have confirmed.[11,29] However, using our ability to incorporate F_nY analogs in place of RNR pathway residues, we have shown that E_{350} is likely not the proton acceptor for Y_{356}, but that its essentiality stems from its involvement in subunit interaction and in the protein conformational gate for RT initiation.[29] The experiments presented herein, the E_{350} studies,[29] the EPR and ENDOR results,[59] and the photo-RNR experiments[35,60] together support fast proton exchange between Y_{356} and solvent via water during PCET across the interface.

Summary. Using site specifically incorporated F_3Y and F_2Y in place of β2 residues 122 and 356, respectively, and taking advantage of the unique EPR features of F_nY• relative to Y•, we have measured the thermodynamic landscape within β2 in the α2β2 complex. These results, when combined with similar types of experiments examining the relative reduction potentials of Y_{356}, Y_{731}, and Y_{730}, provide us with the overall thermodynamic landscape that is uphill by >200 meV and is unprecedented in biology. Why would such a design evolve when other classes of RNRs avoid long-range RT by direct hydrogen atom abstraction from the cysteine by their active cofactors? We propose that the enzyme exerts significant kinetic control over radical initiation. RT in class I RNRs plays a very important role in the fidelity of DNA replication and repair by regulating the relative ratios of the dNDP (and hence dNTP) pools and the absolute amounts of these species. This process is largely controlled by binding the appropriate S/E pairs in α2, 40−50 Å removed from the site of RT initiation by the diferric-Y• cofactor.[48] Subtle changes that occur on S/E binding are thus likely to modulate the reduction potential of residues within the wt RT pathway. All of the experiments conducted to determine the thermodynamic landscape summarized in Figure 8 have been performed with different types of pathway blocks, which are likely to have subtle conformational effects on radical initiation. The proposed uphill nature of the pathway would prevent accumulation of reactive pathway radical intermediates and minimize self-inactivation during the radical initiation process. The connection between our current unprecedented and unexpected thermodynamic measurements and conformational gating of RNR activity by S/E binding is the major focus of our efforts.

■ ASSOCIATED CONTENT

Supporting Information

The Supporting Information is available free of charge on the ACS Publications website at DOI: 10.1021/jacs.6b08200.

Temperature dependence of Y_{356}• formation; temperature-dependent equilibration of F_3Y_{122}• and Y_{356}• in the reaction of F_3Y_{122}•-β2, CDP, ATP, and Y_{731}F-α2 or Y_{730}F-α2; hyperfine values for β-^{1}H and ^{19}F of F_2Y• at different positions on pathway; analysis by method B for one trial of the F_3Y_{122}•-β2/Y_{731}F-α2/CDP/ATP reaction as a function of temperature and one trial of the F_3Y_{122}•-β2/Y_{731}F-α2/CDP/ATP reaction as a function of pH; composite EPR spectra of the F_3Y_{122}•-β2/Y_{731}F-α2/CDP/ATP reaction as a function of temperature (2−15 °C) and the F_3Y_{122}•-β2/Y_{731}F-α2/CDP/ATP reaction as a function of temperature (15−37 °C); temperature dependence of Y_{356}• formation monitored by RFQ-EPR spectroscopy and in the reaction of F_3Y_{122}•-β2/Y_{731}F-α2/CDP/ATP as determined by HQ- and RFQ-EPR

DOI: 10.1021/jacs.6b08200
J. Am. Chem. Soc. 2016, 138, 13706−13716

spectroscopies; temperature-dependent equilibration of F_3Y_{122}• and Y_{356}• in the reaction of F_3Y_{122}•-β2, CDP, ATP, and Y_{731}F-α2 or Y_{730}F-α2; composite EPR spectra of the F_3Y_{122}•-β2/Y_{731}F-α2/CDP/ATP reaction at 25 °C and the F_3Y_{122}•-β2/Y_{731}F-α2/CDP/ATP reaction at 5 °C as a function of pH; pH dependence of Y_{356}• formation in the reaction of F_3Y_{122}•-β2/Y_{731}F-α2/CDP/ATP at 5 °C; reaction of F_2Y_{356}-β2, Y_{731}F-α2, CDP, and ATP monitored by RFQ-EPR spectroscopy (PDF)

AUTHOR INFORMATION

Corresponding Authors

*stubbe@mit.edu

*dnocera@fas.harvard.edu

Present Addresses

K.R.R.: Moderna Therapeutics, 200 Technology Square, Cambridge, MA 02139, United States.

Y.W.: Metabolic Engineering Research Laboratory, 31 Biopolis Way, Nanos #01−01, Singapore 138669.

Notes

The authors declare no competing financial interest.

ACKNOWLEDGMENTS

This work was supported by NIH grants GM29595 (to J.S.), GM47274 (to D.G.N.), and GM079190 (to C.T.). We thank James Mayer for suggesting the pH dependence studies and for helpful discussions regarding the temperature dependence work.

REFERENCES

(1) Thelander, L. *J. Biol. Chem.* **1973**, *248*, 4591−4601.

(2) Brown, N. C.; Reichard, P. *J. Mol. Biol.* **1969**, *46*, 25−38.

(3) Licht, S.; Gerfen, G. J.; Stubbe, J. *Science* **1996**, *271*, 477−81.

(4) Stubbe, J. *Proc. Natl. Acad. Sci. U. S. A.* **1998**, *95*, 2723−4.

(5) Jordan, A.; Reichard, P. *Annu. Rev. Biochem.* **1998**, *67*, 71−98.

(6) Stubbe, J.; van der Donk, W. A. *Chem. Rev.* **1998**, *98*, 705−62.

(7) Nordlund, P.; Reichard, P. *Annu. Rev. Biochem.* **2006**, *75*, 681−706.

(8) Hofer, A.; Crona, M.; Logan, D. T.; Sjöberg, B. M. *Crit. Rev. Biochem. Mol. Biol.* **2012**, *47*, 50−63.

(9) Uhlin, U.; Eklund, H. *Nature* **1994**, *370*, 533−9.

(10) Stubbe, J.; Nocera, D. G.; Yee, C. S.; Chang, M. C. Y. *Chem. Rev.* **2003**, *103*, 2167−201.

(11) Minnihan, E. C.; Nocera, D. G.; Stubbe, J. *Acc. Chem. Res.* **2013**, *46*, 2524−35.

(12) Ekberg, M.; Sahlin, M.; Eriksson, M.; Sjöberg, B. M. *J. Biol. Chem.* **1996**, *271*, 20655−9.

(13) Minnihan, E. C.; Young, D. D.; Schultz, P. G.; Stubbe, J. *J. Am. Chem. Soc.* **2011**, *133*, 15942−5.

(14) Yokoyama, K.; Smith, A. A.; Corzilius, B.; Griffin, R. G.; Stubbe, J. *J. Am. Chem. Soc.* **2011**, *133*, 18420−32.

(15) Yokoyama, K.; Uhlin, U.; Stubbe, J. *J. Am. Chem. Soc.* **2010**, *132*, 8385−97.

(16) Yee, C. S.; Seyedsayamdost, M. R.; Chang, M. C. Y.; Nocera, D. G.; Stubbe, J. *Biochemistry* **2003**, *42*, 14541−52.

(17) Yokoyama, K.; Uhlin, U.; Stubbe, J. *J. Am. Chem. Soc.* **2010**, *132*, 15368−79.

(18) Licht, S.; Stubbe, J. *Compr. Nat. Prod. Chem.* **1999**, *5*, 163−203.

(19) Steenken, S.; Davies, M. J.; Gilbert, B. C. *J. Chem. Soc., Perkin Trans. 2* **1986**, *2*, 1003−10.

(20) Bansal, K. M.; Gratzel, M.; Henglein, A.; Janata, E. *J. Phys. Chem.* **1973**, *77*, 16−9.

(21) Lenz, R.; Giese, B. *J. Am. Chem. Soc.* **1997**, *119*, 2784−94.

(22) Ravichandran, K. R.; Minnihan, E. C.; Wei, Y.; Nocera, D. G.; Stubbe, J. *J. Am. Chem. Soc.* **2015**, *137*, 14387−95.

(23) Ravichandran, K. R.; Liang, L.; Stubbe, J.; Tommos, C. *Biochemistry* **2013**, *52*, 8907−15.

(24) Seyedsayamdost, M. R.; Reece, S. Y.; Nocera, D. G.; Stubbe, J. *J. Am. Chem. Soc.* **2006**, *128*, 1569−79.

(25) Ravichandran, K. R.; Wei, Y.; Taguchi, A. T.; Nocera, D. G.; Stubbe, J.; Tommos, C. Formal reduction potentials of difluorotyrosine and trifluorotyrosine protein residues: Defining the thermodynamics of multistep radical transfer. Unpublished work, **2016**.

(26) Minnihan, E. C.; Seyedsayamdost, M. R.; Uhlin, U.; Stubbe, J. *J. Am. Chem. Soc.* **2011**, *133*, 9430−40.

(27) Chen, H.; Gollnick, P.; Phillips, R. S. *Eur. J. Biochem.* **1995**, *229*, 540−9.

(28) Seyedsayamdost, M. R.; Yee, C. S.; Stubbe, J. *Nat. Protoc.* **2007**, *2*, 1225−35.

(29) Minnihan, E. C. *Mechanistic studies of proton-coupled electron transfer in aminotyrosine- and fluorotyrosine-substituted class Ia ribonucleotide reductase*. Ph.D. Thesis, Massachusetts Institute of Technology, Cambridge MA, June 2012.

(30) Oyala, P. H.; Ravichandran, K. R.; Funk, M. A.; Stucky, P.; Stich, T. A.; Drennan, C. L.; Britt, R. D.; Stubbe, J. *J. Am. Chem. Soc.* **2016**, *138*, 7951−64.

(31) Bollinger, J. M., Jr.; Hangtong, W.; Ravi, N.; Huynh, B. H.; Edmondson, D. E.; Stubbe, J. *Methods Enzymol.* **1995**, *258*, 278−303.

(32) Stoll, S.; Schweiger, A. *J. Magn. Reson.* **2006**, *178*, 42−55.

(33) Orme-Johnson, W. H.; Beinert, H.; Blakley, R. L. *J. Biol. Chem.* **1974**, *249*, 2338−2343.

(34) Olshansky, L.; Pizano, A. A.; Wei, Y.; Stubbe, J.; Nocera, D. G. *J. Am. Chem. Soc.* **2014**, *136*, 16210−6.

(35) Olshansky, L.; Greene, B. L.; Finkbeiner, C.; Stubbe, J.; Nocera, D. G. *Biochemistry* **2016**, *55*, 3234−40.

(36) von Döbeln, U.; Reichard, P. *J. Biol. Chem.* **1976**, *251*, 3616−3622.

(37) Climent, I.; Sjöberg, B. M.; Huang, C. Y. *Biochemistry* **1992**, *31*, 4801−7.

(38) Mao, S. S.; Holler, T. P.; Yu, G. X.; Bollinger, J. M., Jr.; Booker, S.; Johnston, M. I.; Stubbe, J. *Biochemistry* **1992**, *31*, 9733−43.

(39) Booker, S.; Licht, S.; Broderick, J.; Stubbe, J. *Biochemistry* **1994**, *33*, 12676−85.

(40) Wei, Y.; Funk, M. A.; Rosado, L. A.; Baek, J.; Drennan, C. L.; Stubbe, J. *Proc. Natl. Acad. Sci. U. S. A.* **2014**, *111*, E3756−65.

(41) Wei, Y.; Mathies, G.; Yokoyama, K.; Chen, J.; Griffin, R. G.; Stubbe, J. *J. Am. Chem. Soc.* **2014**, *136*, 9001−13.

(42) Mulliez, E.; Fontecave, M.; Gaillard, J.; Reichard, P. *J. Biol. Chem.* **1993**, *268*, 2296−2299.

(43) Ge, J.; Yu, G.; Ator, M. A.; Stubbe, J. *Biochemistry* **2003**, *42*, 10071−83.

(44) Bennati, M.; Robblee, J. H.; Mugnaini, V.; Stubbe, J.; Freed, J. H.; Borbat, P. *J. Am. Chem. Soc.* **2005**, *127*, 15014−5.

(45) Moser, C. C.; Anderson, J. L. R.; Dutton, P. L. *Biochim. Biophys. Acta, Bioenerg.* **2010**, *1797*, 1573−86.

(46) Warren, J. J.; Ener, M. E.; Vlček, A.; Winkler, J. R.; Gray, H. B. *Coord. Chem. Rev.* **2012**, *256*, 2478−2487.

(47) Dutton, P. L.; Page, C. C.; Moser, C. C.; Chen, X. *Nature* **1999**, *402*, 47−52.

(48) Wörsdorfer, B.; Conner, D. A.; Yokoyama, K.; Livada, J.; Seyedsayamdost, M.; Jiang, W.; Silakov, A.; Stubbe, J.; Bollinger, J. M., Jr.; Krebs, C. *J. Am. Chem. Soc.* **2013**, *135*, 8585−93.

(49) Holm, R. H.; Kennepohl, P.; Solomon, E. I. *Chem. Rev.* **1996**, *96*, 2239−314.

(50) Tinberg, C. E.; Lippard, S. J. *Biochemistry* **2009**, *48*, 12145−58.

(51) Berry, B. W.; Martínez-Rivera, M. C.; Tommos, C. *Proc. Natl. Acad. Sci. U. S. A.* **2012**, *109*, 9739−43.

(52) Moser, C. C.; Dutton, P. L. *Biochim. Biophys. Acta, Bioenerg.* **1992**, *1101*, 171−6.

(53) Madej, E.; Wardman, P. *Arch. Biochem. Biophys.* **2007**, *462*, 94−102.

(54) Siegbahn, P. E.; Eriksson, L. A.; Himo, F.; Pavlov, M. *J. Phys. Chem. B* **1998**, *102*, 10622−9.

DOI: 10.1021/jacs.6b08200
J. Am. Chem. Soc. 2016, 138, 13706−13716

(55) Argirević, T.; Riplinger, C.; Stubbe, J.; Neese, F.; Bennati, M. *J. Am. Chem. Soc.* **2012**, *134*, 17661−70.
(56) Zipse, H. *Org. Biomol. Chem.* **2003**, *1*, 692−9.
(57) Pelmenschikov, V.; Cho, K.; Siegbahn, P. E. *J. Comput. Chem.* **2004**, *25*, 311−21.
(58) Bennati, M.; Lendzian, F.; Schmittel, M.; Zipse, H. *Biol. Chem.* **2005**, *386*, 1007−22.
(59) Nick, T.; Lee, W.; Kossmann, S.; Neese, F.; Stubbe, J.; Bennati, M. *J. Am. Chem. Soc.* **2015**, *137*, 289−98.
(60) Olshansky, L.; Stubbe, J.; Nocera, D. G. *J. Am. Chem. Soc.* **2016**, *138*, 1196−205.
(61) Seyedsayamdost, M. R.; Xie, J.; Chan, C. T.; Schultz, P. G.; Stubbe, J. *J. Am. Chem. Soc.* **2007**, *129*, 15060−71.

DOI: 10.1021/jacs.6b08200
J. Am. Chem. Soc. 2016, 138, 13706−13716